Cancer Letters 430 (2018) 133–147

Contents lists available at ScienceDirect

Cancer Letters

journal homepage: www.elsevier.com/locate/canlet

Original Articles

Accelerated lipid catabolism and autophagy are cancer survival mechanisms under inhibited glutaminolysis

Anna Halama[a], Michal Kulinski[b], Shaima S. Dib[a], Shaza B. Zaghlool[a], Kodappully S. Siveen[b], Ahmad Iskandarani[b], Jonas Zierer[c], Kirti S. Prabhu[b], Noothan J. Satheesh[a], Aditya M. Bhagwat[a], Shahab Uddin[b], Gabi Kastenmüller[d], Olivier Elemento[c], Steven S. Gross[e], Karsten Suhre[a,*]

[a] Department of Physiology and Biophysics, Weill Cornell Medicine – Qatar, Education City, PO 24144, Doha, Qatar
[b] Translational Research Institute, Academic Health System, Hamad Medical Corporation, PO 3050, Doha, Qatar
[c] Caryl and Israel Englander Institute for Precision Medicine, Institute for Computational Biomedicine, Sandra and Edward Meyer Cancer Center, Weill Cornell Medicine, New York, NY, USA
[d] Institute of Bioinformatics and Systems Biology, Helmholtz Zentrum München, German Research Center for Environmental Health, 86764, Neuherberg, Germany
[e] Department of Pharmacology, Weill Cornell Medicine, Cornell University, New York, NY, USA

ARTICLE INFO

Keywords:
Cancer metabolism
Glutaminolysis inhibition
Cancer survival mechanisms
Beta-oxidation
Autophagy

ABSTRACT

Suppressing glutaminolysis does not always induce cancer cell death in glutamine dependent tumors because cells may switch to alternative energy sources. To reveal compensatory metabolic pathways, we investigated the metabolome-wide cellular response to inhibited glutaminolysis in cancer cells. Glutaminolysis inhibition with C.968 suppressed cell proliferation but was insufficient to induce cancer cell death. We found that lipid catabolism was activated as a compensation for glutaminolysis inhibition. Accelerated lipid catabolism, together with oxidative stress induced by glutaminolysis inhibition, triggered autophagy. Simultaneously inhibiting glutaminolysis and either beta oxidation with trimetazidine or autophagy with chloroquine both induced cancer cell death. Here we identified metabolic escape mechanisms contributing to cancer cell survival under treatment and we suggest potentially translational strategy for combined cancer therapy, given that chloroquine is an FDA approved drug. Our findings are first to show efficiency of combined inhibition of glutaminolysis and beta oxidation as potential anti-cancer strategy as well as add to the evidence that combined inhibition of glutaminolysis and autophagy may be effective in glutamine-addicted cancers.

1. Introduction

Cancer cells evolve under selective pressure to adjust their metabolism to the high biosynthetic and bioenergetic demands of sustained cell division [1]. The role of cancer-specific metabolic pathways was first identified by Otto Warburg, who reported increased glucose consumption and lactate release in proliferating cancer cells [2]. This picture successively expanded with the identification of further cancer-specific metabolic alterations [1]. For instance, some tumors rely on elevated glutaminolysis to cover their energy needs and fill their carbon and nitrogen pools for the biosynthesis of purines, pyrimidines, non-essential amino acids, and fatty acids [3]. Furthermore, certain lung cancers use branched chain amino acids for protein synthesis and as a source of nitrogen [4]. Recently, lipid catabolism, in particular fatty acid oxidation, was recognized as a further central energy-producing pathway in different cancer types, facilitating proliferation, motility, and metastasis [5–10]. Overall, cancer metabolism appears to be very diverse and driven by intrinsic factors, such as the cancer's genetic makeup, tissue of origin, stage, and grade, as well as extrinsic factors such as the tumor microenvironment or access to oxygen and nutrients. Hence, molecules and processes that contribute to cancer-specific metabolic alterations can serve as targets for therapeutic interventions with the aim of effectively disrupting cancer cell metabolism.

Glutamine metabolism has been envisioned as a therapeutic target against cancer already decades ago [12], but treatment strategies were long unsuccessful due to side effects [3]. Recently, a new generation of compounds targeting glutamine metabolism showed promising results in clinical trials, renewing interest in this therapeutic approach [3]. The enzyme glutaminase catalyzes the conversion of glutamine to glutamate, which is then converted into alpha-ketoglutarate and incorporated into the tricarboxylic acid (TCA) cycle to support the cell's energetic needs [13,14]. In particular, expression of the glutaminase

* Corresponding author. Weill Cornell Medicine - Qatar, Qatar Foundation, Education City, P. O. Box 24144, Doha, Qatar.
E-mail addresses: kas2049@qatar-med.cornell.edu, karsten@suhre.fr (K. Suhre).

https://doi.org/10.1016/j.canlet.2018.05.017
Received 10 February 2018; Received in revised form 25 April 2018; Accepted 12 May 2018

splice variant glutaminase C (GAC) has been associated with a higher glutaminolytic flux in various cancers and indicates glutamine addiction of these cancer cells [15–17]. Among several compounds targeting glutamine metabolism, inhibitors of glutaminase and GAC, namely CB-839 [15] and C.968 [18], respectively, are effective in suppressing proliferation of certain breast cancers and hematological malignancies as well as in inhibiting oncogenic transformation [15,18,19]. However, cancer cell susceptibility to glutamine inhibition can vary among individual cancers. Indeed, treatment for 72 h of breast cancer cell lines with compound CB-839 induces apoptosis in 60% of HCC1806 cells but in only 20% of MB-MDA-231 cells, although growth rates of both cancer cell lines are significantly affected [15]. This finding suggests that certain cancer cells can develop survival mechanisms to overcome nutrient insufficiency, which might further explain limitations of CB-839 as single agent in clinical trial [20,21]. In a clinical setting, such mechanisms can lead to the emergence of resistance. Consequently, uncovering the molecular bases of these metabolic cancer survival mechanisms may contribute to the identification of novel targets that allow for combination therapy and can be tailored to the treatment of specific cancer types.

We hypothesized that survival mechanisms that are activated under inhibited glutaminolysis would be associated with generalized changes in metabolic pathways and that these alterations can be captured and characterized by metabolome-wide profiling. We therefore implemented a broad, non-targeted metabolic profiling approach to identify alterations in cancer metabolism that contribute to cancer cell survival under glutaminolysis inhibition. To the best of our knowledge, metabolome-wide profiling has not been previously used to provide insights into the rewiring of cancer cell metabolism in such settings. So far, previous studies monitored only the impact of glutaminase inhibition by measuring a small set of molecules, i.e., glutamate, glutathione, and TCA cycle intermediates. These studies investigated HCC1806 and T47D cell lines treated with CB-839 [15] and mouse embryonic fibroblasts treated with C.968 [19]. Based on the previous studies in which glutaminolysis inhibition in MB-MDA-231 cell line decreased cell proliferation but was insufficient to trigger apoptosis, we suspected metabolic adaptation in the “glutamine-addicted” MB-MDA-231 cells [15,19]. Therefore, we selected the MB-MDA-231 cell line for our study to identify metabolic “survival mechanisms”. For glutaminolysis inhibition, we used a commercially available, allosteric inhibitor of GAC, compound C.968 [18,19]. This compound effectively suppresses MB-MDA-231 cell proliferation, but its effect on apoptosis, necrosis, and perturbation of the cell cycle have not previously been investigated [18,19]. Here, we investigate cellular processes and metabolic alterations in the MB-MDA-231 cell line under treatment with C.968 at two different dosages and at multiple time points (10 h, 24 h, 48 h, and 72 h). We show that inhibition of glutaminolysis alone does not lead to significant levels of apoptosis, necrosis, or cell cycle arrest. Using broad-range metabolic profiling covering molecules from eight primary pathways including the metabolism of amino acids, carbohydrates, lipids, nucleotides, cofactors, vitamins, peptides, and xenobiotics, we identify accelerated lipid catabolism as an event contributing to survival of glutaminase-inhibited cancer cells. Taken together, the observed alterations in metabolic pathways suggested a critical role for autophagy in cell survival, which we subsequently confirmed. Eventually, we show that simultaneous inhibition of glutaminolysis and either beta oxidation of fatty acids or autophagy increases cell death and thus offers promising treatment options.

2. Materials and methods

2.1. Culture conditions

The established cancer cell line MDA-MB-231 and HCC38 both *in vitro* models for TNBC, were obtained from the American Type Culture Collection (ATCC, Manassas, VA, USA). The established non-small-cell lung cancer cell line NCI-H1838 was obtained from ATCC. All cell lines were grown in Roswell Park Memorial Institute medium (RPMI-1640) (Sigma) supplemented with 10% fetal bovine serum, 1% penicillin–-streptomycin solution (Sigma).

2.2. Experimental design

All experiments for the metabolomics study were performed in a 6-well plate format, and cells from two wells were merged to obtain the appropriate amount of material per single sample. The metabolomics study was performed in duplicates (for each duplicate, cells were harvested from two wells) in three independent experiments (in total six biological replicates were collected per condition). Cells were seeded in the 6-well plate at a density of 0.48×10^6 cells per well. The medium was changed 24 h after seeding with a fresh 4 mL of conditioned media as follows: 1) fresh RPMI medium for control cells; 2) RPMI containing 0.05% of DMSO (vehicle) for control for treatment; 3) RPMI containing 5 μM concentration of C.968; and 4) RPMI containing 10 μM concentration of C.968. The cells were collected at 10 h, 24 h, 48 h, and 72 h after treatment. We used cells treated for 24 h with 1 μM staurosporine as a positive control for apoptosis detection. The cells used for counting and western blot were collected by trypsinization, and the harvesting and processing of cells for metabolite measurement are described below.

2.3. Collection and sample processing for metabolomics

The sample collection was performed as previously described with some modifications [22]. Briefly, the medium was aspirated, and cells were washed twice with 37 °C phosphate-buffered saline (PBS). After PBS was aspirated, 0.5 mL of 80% methanol in H_2O was added per well, and the cells were scraped off from the well to simultaneously quench cellular processes and extract the metabolites. The scraped-in-methanol cells from two wells were combined in one Eppendorf tube (total volume of 1 mL), flash-frozen in liquid nitrogen, and then stored at −80 °C until processing.

The metabolite extraction from the cells was performed in a series of freeze–thaw cycles. All samples were processed simultaneously. The samples were thawed on ice for 5 min with frequent vortexing and afterwards placed in liquid nitrogen for another 5 min. In total, samples underwent a series of three freeze–thaw cycles. After the final freeze–thaw cycle, the cells were centrifuged for 5 min at 18,000 × g at 4 °C. The supernatant was collected into the new tubes, frozen at −80 °C, and shipped to Metabolon Inc. (Durham, NC, USA) on dry ice for metabolite measurements.

To account for differences in cell growth patterns caused by the treatment, the protein content from the pellet that remained after metabolic extraction was determined and used for normalization of the metabolic data. Sample processing for determination of the protein content was performed as previously described [23]. Briefly, pellets were dried in a speed vacuum for 20 min, and 100 μL of 0.2 M NaOH was added to each sample. Samples were heated for 20 min at 95 °C with frequent vortexing and afterwards centrifuged at 18,000 × g for 5 min to remove debris. The protein content was determined using the Bio-Rad DC protein assay, relative to bovine serum albumin standards (0–1.2 mg/mL).

2.4. Non-targeted metabolic profiling

Metabolic profiling was performed using Metabolon platforms deploying Waters ACQUITY ultra-performance liquid chromatography (UPLC) and a Thermo Scientific Q-Exactive high-resolution/accurate mass spectrometer interfaced with a heated electrospray ionization (HESI-II) source and Orbitrap mass analyzer, as previously described [24].

Briefly, recovery standards were added for quality control purposes,

and the extract was divided into the following fractions: 1) two fractions for analysis by two separate reverse-phase (RP)/UPLC-mass spectrometry (MS)/MS methods with positive ion mode electrospray ionization (ESI); 2) one fraction for analysis by RP/UPLC-MS/MS with negative ion mode ESI; 3) one fraction for analysis by hydrophilic interaction chromatography (HILIC)/UPLC-MS/MS with negative ion mode ESI; and 4) one fraction reserved for backup.

The sample extract was dried under nitrogen and reconstituted in solvents compatible with each of the four methods. The aliquots were analyzed in the following conditions: 1) acidic positive ion (optimized for hydrophilic compounds)—extract gradient eluted from a C18 column (Waters UPLC BEH C18–2.1 × 100 mm, 1.7 μm) with water and methanol containing 0.05% perfluoropentanoic acid and 0.1% formic acid; 2) acidic positive ion (optimized for hydrophobic compounds)—extract gradient eluted from C18 (Waters UPLC BEH C18–2.1 × 100 mm, 1.7 μm) with methanol, acetonitrile, water, 0.05% perfluoropentanoic acid, and 0.01% formic acid; 3) basic negative ion—extract gradient eluted from a separate dedicated C18 column using methanol and water containing 6.5 mM ammonium bicarbonate at pH 8; and 4) negative ionization—extract gradient eluted from a HILIC column (Waters UPLC BEH Amide 2.1 × 150 mm, 1.7 μm) using water and acetonitrile with 10 mM ammonium formate at pH 10.8. In the MS analysis, the scan range varied between methods but covered the range of 70–1000 *m/z*.

Metabolon's hardware and software were deployed for raw data extraction, and compounds were identified by comparison of peaks to library entries of purified standards based on retention index, accurate mass match to the library ± 10 ppm, and MS/MS forward and reverse scores between the experimental data and authentic standards. Library matches for each compound were manually checked for each sample. The metabolic data was normalized to correct variations resulting from inter-day tuning differences in the instrument. Each compound was corrected in a run-day. The original metabolic data is available in Supplementary File 1.

2.5. Cell respiration assay

The oxygen consumption rate (OCR) was measured to monitor whether (1) C.968 inhibited glutaminolysis in MDA-MB-231 and (2) fatty acids served as an energy source for MDA-MB-231, using the XF96 extracellular flux analyzer (Seahorse, Agilent). The assay was prepared according to the Seahorse protocols.

To monitor the inhibition of GAC by C.968, the cells were seeded one day before the experiment in the 96-well XF Cell Culture Microplate (Seahorse, Agilent) at a cell density of 15,000 cells/well in RPMI-1640 media (Sigma). The medium was changed, and the cells were treated with vehicle or 10 μM C.968 for 10 h. One hour before the measurements, medium was changed to base medium (Seahorse, Agilent) supplemented with: (1) glucose (10 mM); (2) glutamine (2 mM); or (3) a mixture of glucose and glutamine (10 mM and 2 mM) adjusted to pH 7.4, and the cells were placed in the non-CO_2 incubator for 1 h. The OCR was measured over a period of 80 min after sequential injection of oligomycin (1 μM), FCCP (1 μM), and antimycin A/rotenone (0.5 μM), at time points provided in the manual.

To monitor the cells' ability to use fatty acids, the cells were seeded in 96-well XF Cell Culture Microplate (Seahorse, Agilent) at a cell density of 15,000 cells/well in growth medium RPMI-1640 (Sigma) and cultivated for 24 h. The medium was replaced with a base medium (Seahorse, Agilent) supplemented with 0.5 mM glucose, 1 mM GlutaMAX, 0.5 mM carnitine, and 1% fetal bovine serum, and the cells were cultivated for 24 h. At 1 h before the measurements, cells were washed once with Krebs–Henseleit buffer (111 mM NaCl, 4.7 mM KCl, 1.25 mM $CaCl_2$, 2 mM $MgSO_4$, 1.2 mM NaH_2PO_4, 2.5 mM) supplemented with glucose, 0.5 mM carnitine, and 5 mM HEPES and incubated in the same media for 45 min in the non-CO_2 incubator. 20 min prior to the measurements, etomoxir (40 μM) or DMSO was added to the wells, and cells were incubated for next 15 min. Right before taking the measurements, XF Palmitate-BSA FAO substrate was added to the wells. The oxygen consumption rate was measured over a period of 80 min after sequential injection of oligomycin (1 μM), FCCP (1 μM), and antimycin A/rotenone (0.5 μM), at the time points provided in the manual.

2.6. Western blotting

Whole cell lysates were prepared in a 20 mM Tris-HCL lysis buffer (pH 7.49) supplemented with protease–phosphatase cocktail inhibitors (Roche) and phenyl methane sulfonyl fluoride (Sigma Aldrich). Samples were lysed by three freeze–thaw cycles in liquid nitrogen as previously described [25]. The supernatant was collected after centrifugation for 10 min, and the total protein content was quantified using the DC protein assay (Bio-Rad). The proteins were denatured by incubation with 4 × Laemmli buffer at 95 °C for 10 min.

Gel electrophoresis was performed using the prepared whole cell lysate and transferred to a polyvinylidene fluoride membrane (Bio-Rad). The membrane was blocked in 5% milk solution in Tween-PBS (PBS with 0.1% Tween 20) for 1 h and incubated overnight in a primary antibody at 4 °C. The overnight incubation was followed by three washing steps in Tween-PBS. The membrane was incubated in the corresponding secondary antibody followed by three washing steps. Both primary and secondary antibodies were prepared in the recommended dilution in a 5% milk solution in Tween-PBS. The blots were developed and visualized under a ChemiDoc system (Amersham, Bio-Rad, USA). The primary antibodies used were CPT1a (Cell Signaling, #12252S),CPT2 (Santa Cruz, #sc-377294), LC3A/B (Cell Signaling, #4108s), Cleaved Caspase-3 (Cell Signaling, #9661L), GAPDH (Santa Cruz, #sc-25778), (Santa Cruz, #sc-81178). The corresponding secondary antibodies included horseradish peroxidase–conjugated anti-mouse (Cell Signaling) and anti-rabbit (Cell Signaling).

2.7. Cell cycle monitoring

MDA-MB-231 cells were exposed to two different concentrations of C.968 (5 μM and 10 μM) for 10 h, 24 h, 48 h, and 72 h. Cells were washed, fixed with 70% ethanol, and incubated for 30 min at 37 °C with 0.1% RNase A in PBS. Cells were washed again, resuspended, and stained with 25 μg/mL PI for 30 min in PBS at room temperature. The cell distribution across the cell cycle was analyzed by flow cytometry using a BD LSRFortessa analyzer (BD Biosciences) as previously described [26].

2.8. Cell death monitoring

MDA-MB-231 cells were exposed to two different concentrations of C.968 (5 μM and 10 μM) for 10 h, 24 h, 48 h, and 72 h. The cells were collected by trypsinization, washed with PBS, and stained with fluorescein-conjugated annexin V and PI (BD Biosciences). The percentage of cells undergoing apoptosis or necrosis was measured by flow cytometry using a BD LSRFortessa analyzer (BD Biosciences) as previously described [27]. The cell viability status was quantified based on the staining as follows: the live (Annexin-$FITC^-$negative, PI^- negative), early apoptosis (Annexin-$FITC^+$positive, PI^-negative), late apoptosis (Annexin-$FITC^+$ positive, PI^+ positive) apoptotic cells, and necrosis (Annexin-$FITC^-$negative, PI^+positive).

2.9. Statistical analysis

Statistical analysis was performed in R version 3.1.3 and R-Studio version 0.97.551. The metabolomics data were normalized to protein content, followed by log transformation and z-scoring.

Multivariate linear regression was used to assess the statistical

significance of the association of metabolites with C.968 treatment in MDA-MB-231 over the entire course of the experiment while adjusting for time. Additionally, we used linear regression to test the association of metabolites with the C.968 treatment in MDA-MB-231 cells at specific time points separately (10 h, 24 h, 48 h, and 72 h). Significance was defined at a stringent Bonferroni level of $p < 1.44 \times 10^{-04}$ ($p < 0.05/346$).

We also performed analysis of ratios between metabolites because using ratios reduces the overall variance and allows for identification of biologically relevant pathways, as previously reported [28,29]. We examined the time-resolved effect of the C.968 treatment on metabolite ratios in MDA-MB-231 cells, using a multivariate linear regression model for each pair of metabolites. In total, we calculated 59,685 metabolic ratios (346 × 345/2). We considered metabolite ratios as significantly altered if they satisfied both the following conditions: p-value $< 8.37 \times 10^{-07}$ ($p < 0.05/59,685$) and p-gain define measure to identify statistically significant metabolite ratios [29] $> 5.96 \times 10^{05}$ (p-gain $> 10 \times 59,685$).

The Orthogonal Projections to Latent Structures (OPLS) analysis using time and drug dose as phenotype was performed with SIMCA version 14 (Umetrics, Umea, Sweden).

3. Results

3.1. Glutaminase inhibition reduces cell proliferation but does not trigger apoptosis or cell cycle arrest

In previous studies, C.968 was reported to be a potential glutaminolysis inhibitor in the GAC-expressing triple-negative breast cancer (TNBC) cell line MDA-MB-231 [18,19,30]. Thus, Our first objective was to verify that compound C.968 effectively inhibits glutaminolysis in our experimental set-up. The presence of GAC protein in the MDA-MB-231 cell line was determined using western blot (Supplementary Fig. 1 A). Glutaminase catalyzes the transformation of glutamine to glutamate, which is then which is then converted into alpha-ketoglutarate and incorporated into the TCA cycle to support cellular energetic needs [14]. The inhibition of GAC is expected to reduce the amount of available substrate for oxidation, and a decreased oxygen consumption rate (OCR) under inhibited glutaminolysis thus is expected. We used OCR as the readout for monitoring mitochondrial respiration in the MDA-MB-231 cell line. Toward this end, we quantified OCR in the MDA-MB-231 cells that were treated with either vehicle or 10 μM C.968 after incubation in a conditioned medium supplemented with the following alternative bioenergetics substrates: 1) a combination of glucose plus glutamine; 2) glutamine only; or 3) glucose only. We observed a decrease in OCR in cells treated with C.968 in a medium supplemented with glutamine only, as well as in glucose-plus-glutamine medium, but not in medium supplemented with glucose (Fig. 1A). The observation of higher OCR in the untreated cells in medium containing glutamine vs. glucose indicates that MDA-MB-231 cells rely on glutamine as their principal mitochondrial fuel source, in agreement with a previous report suggesting the addiction of TNBC to glutamine [15]. Treatment-resulted decrease in OCR of MDA-MB- 231 cells cultivated in media supplemented with glutamine as a single agent further indicated that C.968 has inhibited glutaminolysis in this cell line.

Previous studies have also shown that C.968 effectively suppresses proliferation of MDA-MB-231 cells [18]. Thus, we monitored the impact of C.968 on MDA-MB-231 cell proliferation over a period of 72 h at multiple time points (10 h, 24 h, 48 h, and 72 h). Treatment with C.968 resulted in a time- and dose-dependent decrease in cell number (Fig. 1B), in agreement with previous findings [18]. A significant decrease in cell number together with morphological changes, namely from a fibroblast-like structure to spherical, was further observed by microscopy investigation, with the largest effect after 72 h of treatment (Supplementary Fig. 1 B).

We next asked whether the observed decrease in MDA-MB-231 cell number after treatment with C.968 is due to cell apoptosis or necrosis because another glutaminase inhibitor, CB-839, was reported to induce an apoptotic response in only 20% of an MDA-MB-231 cell population [15]. Accordingly, we quantified apoptosis in the MDA-MB-231 cells over a period of 72 h at different time points by monitoring both the caspase 3 cleavage and Annexin V/propidium iodide (PI) cell membrane dual staining. Neither cleavage of caspase 3 nor Annexin V/PI dual staining was observed within the range of C.968 concentrations used, suggesting no apoptosis in glutaminase-inhibited MB-MDA-231 cells over a 72-h period (Fig. 1C and D). In agreement with a previous study [15], we observed late apoptosis in less than 20% of cells at 48 h and 72 h after C.968 treatment (Fig. 1D). Using DAPI staining, we further confirmed the absence of apoptosis after treatment (Supplementary Fig. 2), using Annexin V/PI dual staining we excluded necrosis (Fig. 1D). We also monitored the MB-MDA-231 cells over prolonged experimental period of 7 days under inhibited glutaminolysis and we have not observed increase in apoptosis as indicated by DAPI staining (Supplementary Fig. 2B).

As decreased cell proliferation could result from perturbations of the cell cycle, we investigated whether the observed decrease in cell number was associated with cell cycle arrest. We characterized the cell cycle of C.968-treated MB-MDA-231 cells and observed no differences in the cell cycle between treated and untreated cells at 10 h and 24 h after treatment (Fig. 1E), when the majority of the cell population was in the G0/G1 phase. The population of cells in the sub-G0 phase was found to increase 72 h after treatment (from 2.42% in vehicle-treated cells to 6.68% in cells treated with 10 μM C.968), with a simultaneous decrease in G2/M phase (from 8.85% in vehicle-treated cells to 4.78% in cells treated with 10 μM C.968). Taken together, we showed that treatment with C.968 suppresses proliferation of MB-MDA-231 cells but does not induce apoptosis or lead to substantial cell cycle arrest.

3.2. Signatures of metabolic adjustment of MB-MDA-231 cells after glutaminolysis inhibition

Because C.968 treatment reduced proliferation, but was insufficient to induce cell death, we hypothesized that inhibition of glutaminolysis in MB-MDA-231 cells triggered a metabolic compensation mechanism that enabled the cells to survive under substrate-limiting conditions (Fig. 1). We therefore conducted non-targeted metabolic profiling to obtain a readout of metabolic changes associated with cell responses to C.968 treatment. Using the Metabolon platform [24], we quantified relative levels of 346 distinct metabolites for untreated MB-MDA-231 cells as well as those treated with dimethyl sulfoxide (DMSO) (vehicle) and with C.968 at 5 μM and 10 μM for time points of 10 h, 24 h, 48 h and 72 h. The identified metabolites cover molecules from eight primary pathways related to the transformation of amino acids, carbohydrates, cofactors and vitamins, energy, lipids, nucleotides, peptides, and xenobiotics (Supplementary Table 1). Treatment of MB-MDA-231 cells with C.968 resulted in time- and dose-dependent alterations in cell metabolism, as revealed by Orthogonal Projections to Latent Structures (OPLS) regression modeling (Fig. 2A). The biological replicates clustered tightly together and separated by dosage and duration of treatment. Untreated and vehicle-treated cells grouped together, suggesting only minor effects of DMSO at vehicle concentration (Supplementary Table 2). A clear separation of cells treated with 5 μM and 10 μM C.968 and location of the 5 μM cluster between the DMSO and the 10 μM clusters indicated a dose-dependent impact of glutaminase inhibition on the global metabolic profiles. A distinct separation between the time points and their chronological order indicated that progressive metabolic changes induced by glutaminase inhibition took place over time. The corresponding loading plots allowed for identification of those metabolites that contributed most to the separation of these groups, i.e., metabolites aligned with the dosage direction and with the temporal direction in these plots are those of interest for the respective factor (Fig. 2B). The loading plot thus suggests that

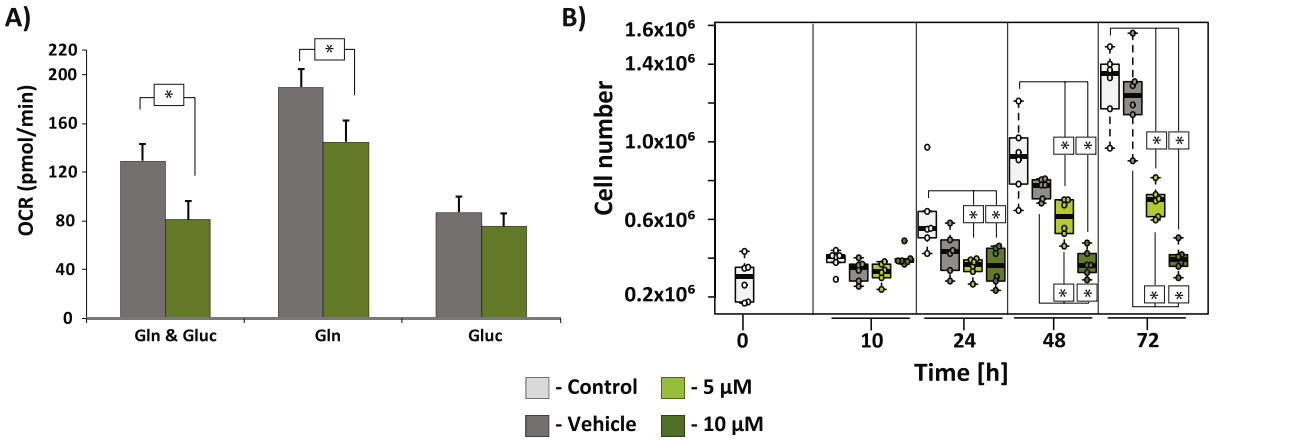

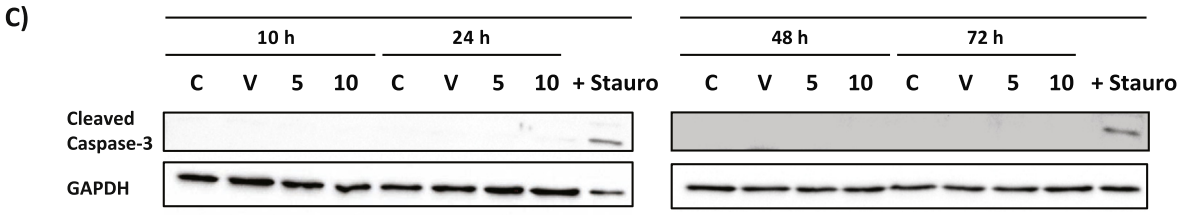

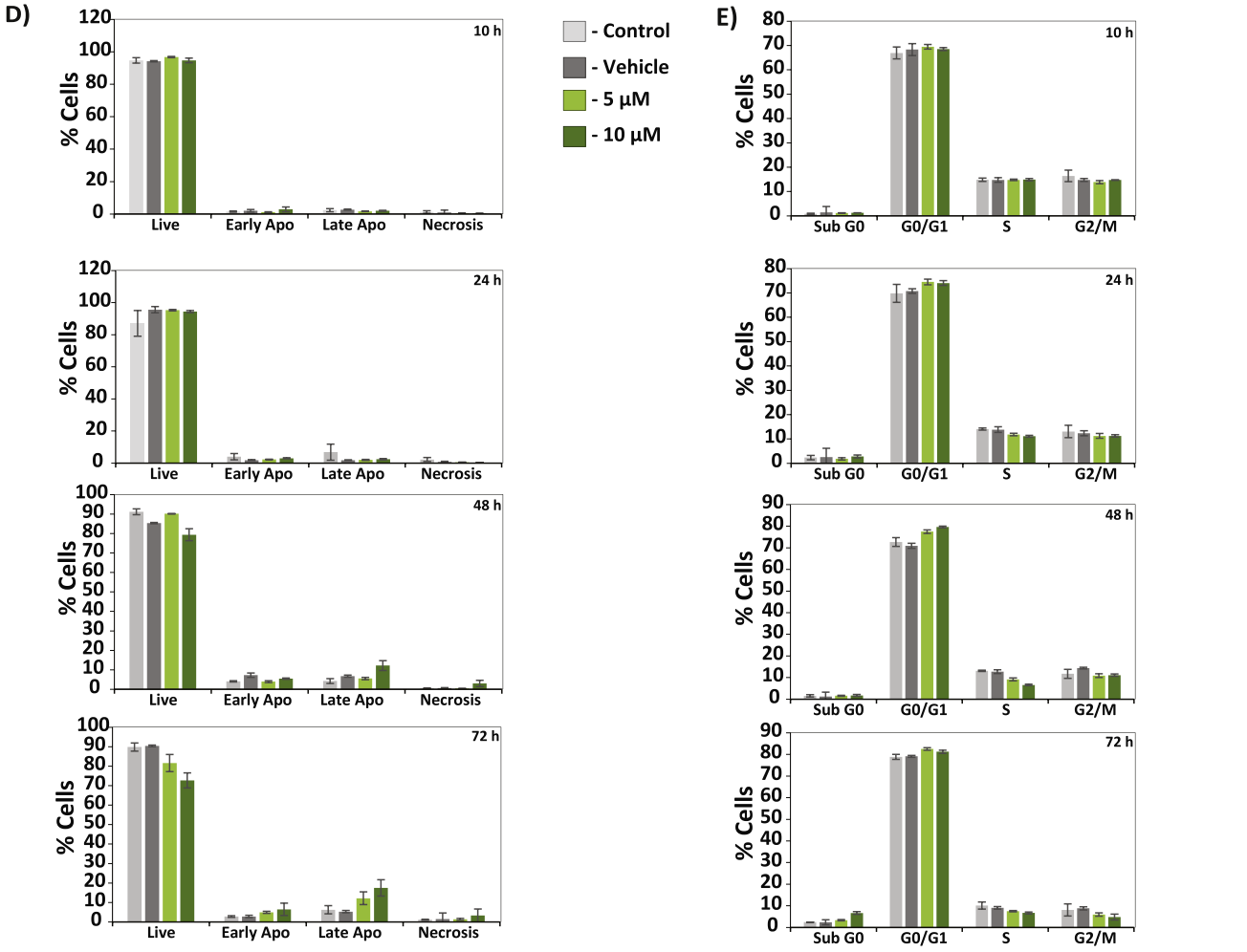

(caption on next page)

Fig. 1. C.968 inhibits proliferation of MDA-MB231 cells but does not induce apoptosis or cell cycle arrest. A) Oxygen consumption rate (OCR) was determined in cells treated with vehicle or 10 μM C.968 after cell incubation in media containing: 1) mixture of glutamine and glucose (Gln & Gluc); 2) glutamine only (Gln); or 3) glucose only (Gluc). **B)** Cell number was determined in untreated cells or cells treated with vehicle or C.968 (5 μM and 10 μM) over 72 h. **C)** Western blotting analysis for cleaved caspase-3. **D)** Apoptosis and necrosis were not induced by treatment with C.968 as determined after staining of cells with fluorescein-conjugated annexin-V and propidium iodide (PI) and analysis with flow cytometry. **E)** No changes in cell cycle were observed after treatment, as shown by PI staining and analysis for DNA content by flow cytometry. *p < 0.01; untreated cells are depicted in white, vehicle-treated in grey, and treated with 5 μM or 10 μM C.968 in green and dark green, respectively.

molecules involved in metabolism of lipids, amino acids, and nucleotides were the major contributors to this separation of dosage clusters.

To uncover metabolic alterations that are significant after treatment of the MB-MDA-231 cells with C.968, we applied a linear regression model between the metabolite levels and the dosage of C.968, using time as a covariate. We identified 82 metabolite associations that exhibit a stringent Bonferroni-corrected p-value ($p \leq 1.44 \times 10^{-4}$, corresponding to an alpha error significance level of $p \leq 0.05$ after accounting for 346 tests) (Table 1). Most molecules with significantly changed levels were involved in the metabolism of lipids (38 molecules) and amino acids (21 molecules).

The metabolic response of MB-MDA-231 cells to C.968 treatment progressed over time. During the first 10 h after treatment, only 6 metabolites were significantly altered, all lipid metabolism intermediates. After 24 h of C.968 treatment, the number of significantly altered metabolites increased to 24 molecules, involved in the metabolism of lipids, amino acids, carbohydrates, and nucleotides. We observed significant alterations in 44 and 58 metabolites after 48 h and 72 h of treatment, respectively. Although the altered metabolites were from different metabolic classes at these later time points, the

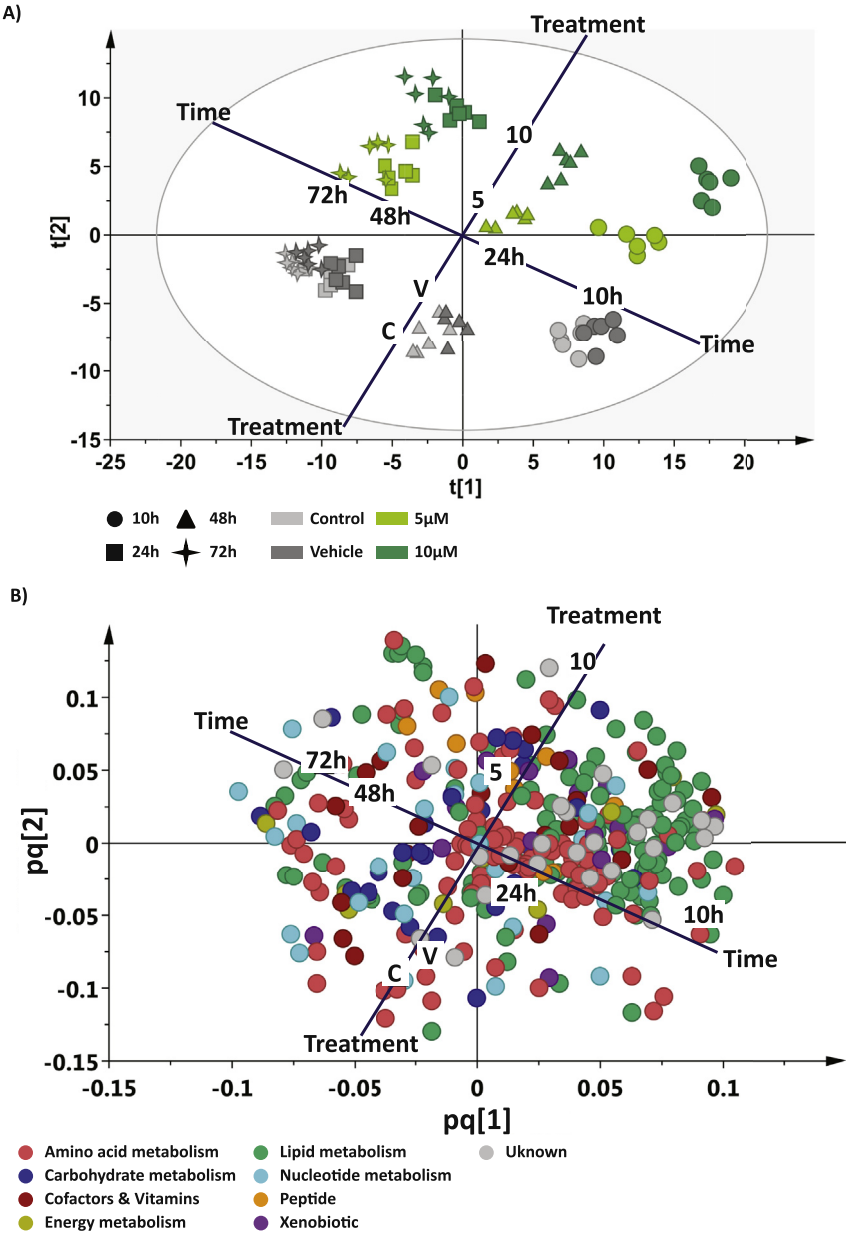

Fig. 2. Inhibition of glutaminolysis with C.968 causes general metabolic adjustments. A) OPLS reveals time- and dose-dependent separation between groups. **B)** OPLS loading plot shows contribution of different metabolic classes to the separation.

Table 1
Metabolites altered in C.968-treated MDA-MB-231 cells.

Metabolite	Trend	Pathway	Time	10 h	24 h	48 h	72 h
Phenylacetylglycine	↑	**Amino acid**	1.29×10^{-14}			9.80×10^{-06}	3.22×10^{-07}
Isovalerylcarnitine	↓		1.29×10^{-12}			4.07×10^{-06}	2.80×10^{-07}
Cysteinylglycine	↓		7.37×10^{-12}		5.66×10^{-05}	4.80×10^{-05}	5.86×10^{-08}
Putrescine	↓		6.64×10^{-11}		6.85×10^{-06}	8.81×10^{-08}	1.58×10^{-07}
2-methylbutyrylcarnitine (C5)	↓		2.31×10^{-10}				2.75×10^{-06}
Phenol sulfate	↑		4.04×10^{-10}			2.80×10^{-05}	1.15×10^{-05}
Glutathione, reduced (GSH)	↓		5.17×10^{-10}		4.12×10^{-05}		8.32×10^{-05}
4-imidazoleacetate	↑		1.34×10^{-09}			2.25×10^{-05}	
N-acetylthreonine	↑		4.91×10^{-08}				
S-methylglutathione	↓		9.04×10^{-08}				
N-acetylputrescine	↓		5.11×10^{-07}			1.02×10^{-05}	2.13×10^{-05}
4-hydroxy-nonenal-glutathione	↑		1.17×10^{-06}				
3-(4-hydroxyphenyl)lactate	↑		1.29×10^{-06}				
S-adenosylhomocysteine (SAH)	↓		2.71×10^{-06}				
Hypotaurine	↓		9.03×10^{-06}				1.46×10^{-07}
5-hydroxyindoleacetate	↑		1.30×10^{-05}				
Isobutyrylcarnitine	↓		2.08×10^{-05}				3.40×10^{-05}
N-acetylalanine	↑		2.30×10^{-05}				
Carboxyethyl-GABA	↑		6.89×10^{-05}				
Creatine phosphate	↓		8.95×10^{-05}				3.22×10^{-06}
N-acetylphenylalanine	↑		1.10×10^{-04}				
Imidazole lactate	↓						2.11×10^{-13}
Ethylmalonate	↓						4.32×10^{-05}
N6,N6,N6-trimethyllysine	↑					8.72×10^{-05}	
N-acetylmethionine	↓						3.84×10^{-05}
Methionine	↑					2.38×10^{-05}	7.85×10^{-05}
Arginine	↓						1.92×10^{-05}
Erythronate	↑	**Carbohydrate**	1.24×10^{-10}		9.93×10^{-05}		
Glucuronate	↓		2.05×10^{-06}			2.34×10^{-05}	6.17×10^{-06}
Ribitol	↑		1.64×10^{-05}				
Galactonate	↓						3.19×10^{-17}
Mannitol/sorbitol	↑				1.13×10^{-04}		
Pyruvate	↓						3.20×10^{-06}
1-methylnicotinamide	↑	**Cofactors and Vitamins**	8.28×10^{-11}			9.36×10^{-07}	
Nicotinamide riboside	↑		7.37×10^{-10}			5.59×10^{-05}	
Pantothenate	↑		1.76×10^{-08}				
Gulonic acid	↓		5.66×10^{-06}				1.88×10^{-08}
Coenzyme A	↓		3.12×10^{-05}				2.73×10^{-05}
Pyridoxal phosphate	↓						3.43×10^{-15}
Phosphate	↑		1.53×10^{-09}			5.46×10^{-09}	2.55×10^{-07}
2-methylcitrate/homocitrate	↑	**Energy**	4.80×10^{-06}				2.56×10^{-05}
Fumarate	↓						1.45×10^{-05}
Alpha-ketoglutarate	↓						1.25×10^{-05}

(*continued on next page*)

Table 1 (*continued*)

Metabolite	Trend	Pathway	Time	10 h	24 h	48 h	72 h
Stearoylcarnitine	↑	**Lipid**	1.42×10^{-25}	2.38×10^{-06}	1.30×10^{-10}	4.12×10^{-10}	9.80×10^{-09}
Oleoylcarnitine	↑		5.68×10^{-19}	1.14×10^{-04}	1.11×10^{-08}	1.44×10^{-08}	3.30×10^{-08}
Phosphoethanolamine	↑		1.24×10^{-16}	6.43×10^{-08}	2.20×10^{-08}	6.32×10^{-06}	2.86×10^{-06}
1-oleoyl-GPI (18:1)	↑		2.01×10^{-15}		2.50×10^{-05}	2.71×10^{-08}	
Glycerophosphoethanolamine	↓		5.39×10^{-15}		4.30×10^{-06}	3.46×10^{-05}	1.67×10^{-07}
3-hydroxy-3-methylglutarate	↑		1.68×10^{-14}		5.01×10^{-05}	1.42×10^{-06}	2.53×10^{-07}
Palmitoylcarnitine	↑		3.48×10^{-11}	3.97×10^{-05}	1.36×10^{-07}	1.39×10^{-06}	3.75×10^{-05}
Palmitoleoylcarnitine	↑		3.95×10^{-11}		6.29×10^{-08}	1.45×10^{-05}	1.23×10^{-04}
Acetyl CoA	↑		5.67×10^{-11}				
Lactosyl-N-palmitoyl-sphingosine	↑		1.43×10^{-10}			8.83×10^{-06}	
1,2-dioleoyl-GPI (18:1/18:1)	↑		2.02×10^{-10}			3.26×10^{-06}	6.01×10^{-05}
1-stearoyl-GPC (18:0)	↑		2.56×10^{-10}			3.07×10^{-05}	
Laurylcarnitine	↑		2.86×10^{-10}		2.56×10^{-07}	2.22×10^{-05}	
Myristoylcarnitine	↑		5.23×10^{-10}	5.32×10^{-05}	4.29×10^{-08}	1.03×10^{-07}	
1-stearoyl-2-oleoyl-GPI (18:0/18:1)	↑		6.51×10^{-10}			4.47×10^{-06}	2.18×10^{-05}
1-palmitoyl-GPC (16:0)	↑		8.06×10^{-10}			1.24×10^{-04}	
1-linoleoyl-GPC (18:2)	↑		5.69×10^{-09}			1.34×10^{-06}	
Eicosapentaenoate (EPA; 20:5n3)	↑		1.16×10^{-08}			1.45×10^{-06}	1.99×10^{-05}
1-oleoyl-GPC (18:1)	↑		1.88×10^{-08}			3.27×10^{-05}	1.25 × 10-04
1-stearoyl-GPI (18:0)	↑		3.24×10^{-08}				
1-oleoyl-GPS (18:1)	↑		4.45×10^{-08}		1.23×10^{-04}	1.74×10^{-05}	
Sphingosine	↑		4.99×10^{-08}			3.85×10^{-09}	1.05×10^{-04}
Choline phosphate	↑		1.45×10^{-07}				3.56×10^{-05}
Myristoleoylcarnitine	↑		1.46×10^{-07}		1.14×10^{-05}		
Oleamide	↑		1.60×10^{-07}				
1-arachidonoyl-GPC (20:4n6)	↑		2.07×10^{-07}			1.19×10^{-04}	
1-palmitoleoyl-GPC (16:1)	↑		4.27×10^{-07}		8.31×10^{-05}		
1-palmitoyl-2-oleoyl-GPG (16:0/18:1)	↓		4.99×10^{-07}				
1-stearoyl-2-arachidonoyl-GPS (18:0/20:4)	↑		5.45×10^{-06}				
Glycerophosphoglycerol	↓		6.24×10^{-06}				3.76×10^{-07}
Docosahexaenoate (DHA; 22:6n3)	↑		6.88×10^{-06}			3.79×10^{-06}	3.19×10^{-06}
Glycerophosphorylcholine (GPC)	↓		7.21×10^{-06}	1.49×10^{-05}	8.94×10^{-06}		
1-stearoyl-2-arachidonoyl-GPI (18:0/20:4)	↑		2.03×10^{-05}				
2-palmitoyl-GPC (16:0)	↑		2.54×10^{-05}				
1-lignoceroyl-GPC (24:0)	↑		3.61×10^{-05}		5.37×10^{-15}	2.03×10^{-08}	3.66×10^{-06}
Palmitic amide	↑		5.16×10^{-05}				3.19×10^{-06}
Arachidonate (20:4n6)	↑		9.90×10^{-05}				8.63×10^{-06}
Cytidine 5′-diphosphocholine	↑		1.08×10^{-04}				
Butyrylcarnitine	↓						7.36×10^{-07}
1-arachidonoyl-GPE (20:4n6)	↑						8.76×10^{-06}
1-arachidonoyl-GPI (20:4)	↑				3.60×10^{-05}	2.03×10^{-07}	3.75×10^{-05}
1-palmitoylglycerol (16:0)	↑						2.59×10^{-05}
N-carbamoylaspartate	↓	**Nucleotide**	4.31×10^{-09}		6.11×10^{-05}	6.08×10^{-07}	4.56×10^{-06}
Orotate	↓		2.40×10^{-07}		5.27×10^{-05}	8.89×10^{-08}	9.33×10^{-05}
Cytidine diphosphate	↓		6.97×10^{-07}				2.03×10^{-05}
Uridine	↑		9.51×10^{-06}				
Urate	↑		4.75×10^{-05}				
Guanosine	↑		1.44×10^{-04}				
Gamma-glutamyl-epsilon-lysine	↑	**Peptide**	3.20×10^{-06}			4.53×10^{-06}	
Gamma-glutamylglutamate	↑		3.59×10^{-06}			9.78×10^{-05}	
Salicylate	↑	**Xenobiotics**	2.38×10^{-07}			5.16×10^{-06}	3.68×10^{-06}
Phenol red	↑		9.61×10^{-07}		1.38×10^{-04}	3.27×10^{-05}	2.70×10^{-07}
Ergothioneine	↓		6.73×10^{-06}			4.04×10^{-07}	1.02×10^{-12}
Trizma acetate	↑		1.49×10^{-05}				
Myristoyl sulfate	↑		1.38×10^{-04}				
HEPES	↑						8.56×10^{-06}
Gluconate	↓						5.28×10^{-05}
Beta-guanidinopropanoate	↓						1.29×10^{-05}

The direction of metabolic alterations is represented by arrows (↓ - decrease; ↑ - increase). "Time" and time intervals (10 h, 24 h, 48 h, and 72 h) reflect metabolites showing significant alteration over the entire experimental period and at specific time points (relative to vehicle), respectively. The p-vale was calculated from a linear regression model between the metabolite and dose of C.968, with time as a covariate. The p-value reflects changes in significance observed after cell treatment with 10 μM drug concentration over time.

predominately observed changes were with molecules involved in lipid and amino acid metabolism. These findings suggest that inhibition of glutaminolysis predominantly affects lipid and amino acid metabolism, indicating a central role for these molecules in the metabolic adjustment to GAC inhibition.

3.3. TCA cycle intermediates, but not glutamate, decrease with inhibition of glutaminolysis

Inhibition of GAC would be expected to cause a decrease in glutamate level if this pathway would be the single cellular source of glutamate. In a previous study, inhibition of GAC with C.968 in mouse embryonic fibroblasts resulted however in no significant depletion of

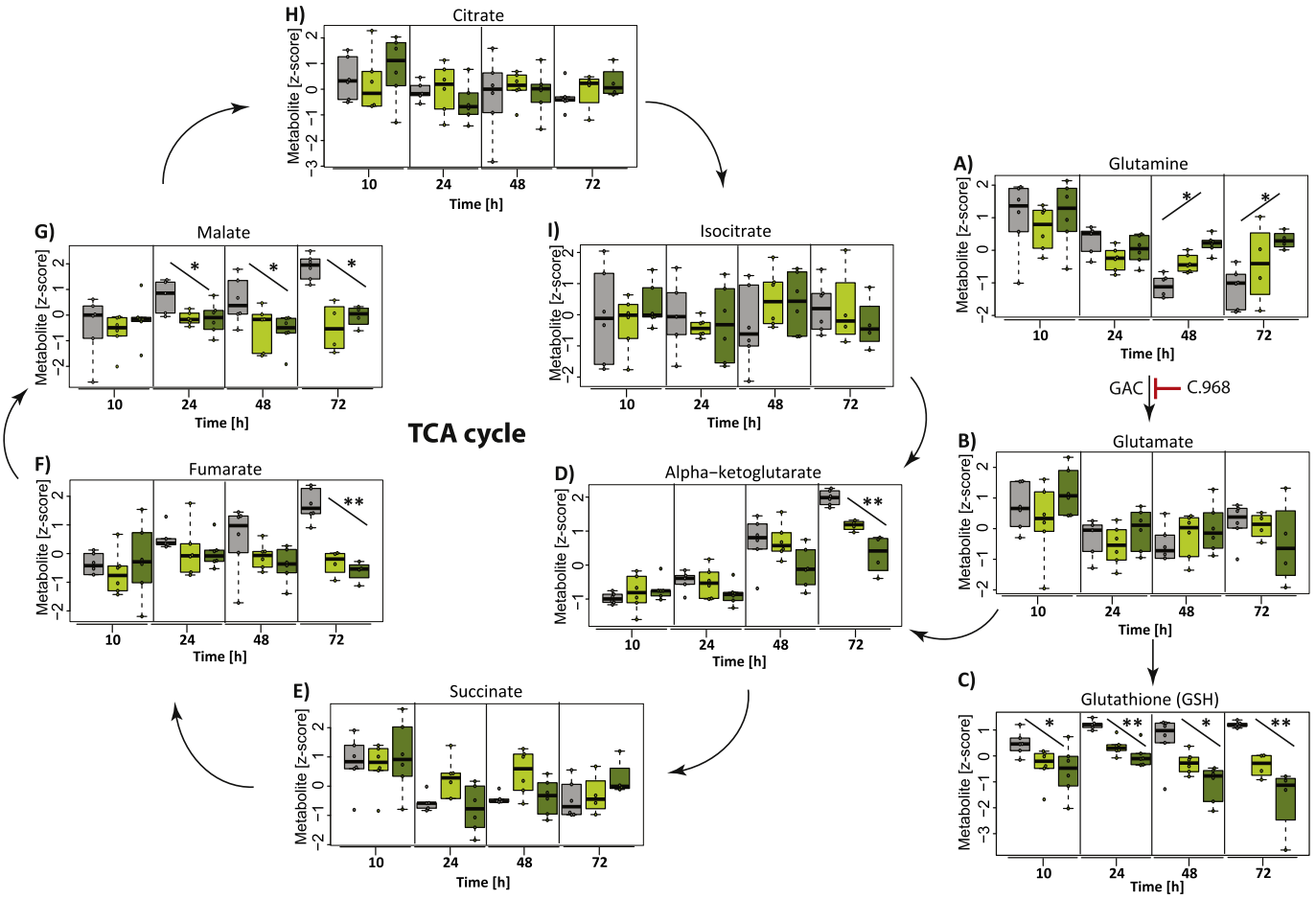

Fig. 3. Impact of glutaminase inhibition on the glutamate pool and TCA cycle metabolism. The boxplots present alteration patterns of glutamine, glutamate, reduced glutathione, and TCA cycle intermediates after treatment of cells with C.968. Vehicle-treated cells are depicted in grey, and those treated with 5 μM or 10 μM C.968 are indicated by green and dark green, respectively. ** indicates Bonferroni-corrected significant (p-value $\leq 1.35 \times 10^{-04}$) changes; * indicates trend (p-value ≤ 0.05).

glutamate and TCA cycle intermediate levels [19]. In the same study the authors showed significant decrease in ^{13}C isotopic enrichment from [U-^{13}C]-glutamine after treatment with C.968, which further suggests that GAC inhibition is not critical for the overall glutamate pool [19]. In agreement with these observations, we found a slight increase in glutamine levels (Fig. 3 A) with C.968 treatment, but no significant changes in glutamate levels (Fig. 3 B). However, we observed a significant decrease in glutathione (Fig. 3C) and TCA cycle intermediates at 72 h after treatment, including alpha-ketoglutarate, the direct metabolic product of glutamate, along with fumarate and malate (Fig. 3 D, E, and F). Other TCA cycle intermediates (citrate, isocitrate, and succinate) were unchanged by GAC inhibition (Fig. 3 G, H, and I). A decrease in TCA cycle intermediates without significant changes in glutamate level suggests that glutamate metabolism, rather than absolute glutamate levels, was altered by GAC inhibition in the MB-MDA-231 cell line. These observations indicate that alternative metabolic pathways were activated to compensate for the loss of glutamate and consequent TCA cycle intermediates depletion.

3.4. Lipid catabolism accelerates as a response to glutaminolysis inhibition

As we have previously shown, associations with ratios between metabolite levels can reveal biochemical pathways and reduce variance within the experimental data [29]. To identify metabolites directly affected by treatment of MB-MDA-231 cells with C.968, we therefore calculated metabolic ratios of glutamate relative to all other quantified metabolites. This analysis revealed significant increases (p-value $\leq 8.37 \times 10^{-7}$; p-gain $\geq 5.96 \times 10^{5}$) in the ratios of glutamate vs. stearoylcarnitine, oleoylcarnitine, 1-oleoyl-GPI (18:1), and 1-methylnicotinamide (Fig. 4). Of note, all four of these metabolites contribute to lipid metabolism: acyl-carnitines are modified fatty acids for traffic across the inner mitochondrial membrane; glycophosphoinositols are lipid species involved in cell structure and signaling processes; and 1-methylnicotinamide is a product of the metabolism of NAD/NADP that contributes to *de novo* lipid biosynthesis and cellular antioxidant defenses. These results suggest the potential involvement of accelerated lipid metabolism as a compensatory response of cancer cells after GAC inhibition.

Thus, we further focused on molecules involved in lipid metabolism, showing significant alterations after glutaminolysis inhibition in the MB-MDA-231 cell line. Of note, GAC inhibition resulted in increased levels of lysophospholipids and polyunsaturated fatty acids (PUFA), concomitant with decreases in glycerophosphorylcholine (GPC) and phosphoethanolamines (Supplementary Fig. 3). These alterations suggest accelerated catabolism of glycerophospholipids. Furthermore, the observed increase in monoacylglycerols suggests accelerated degradation of triacylglycerols and/or diacylglycerols, resulting in the release of fatty acids for ATP generation via beta-oxidation. In accord with this possibility, we observed significant increases in acyl-carnitines, known to deliver fatty acids to the mitochondria for beta-oxidation (Supplementary Fig. 3). Also, levels of stearoyl-carnitine, palmitoyl-carnitine, myristoyl-carnitine, and oleoyl-carnitine all significantly increased at 10 h after C.968 treatment, followed by significant increases in palmitoleoyl-carnitine, lauryl-carnitine, and myristoleoyl-carnitine

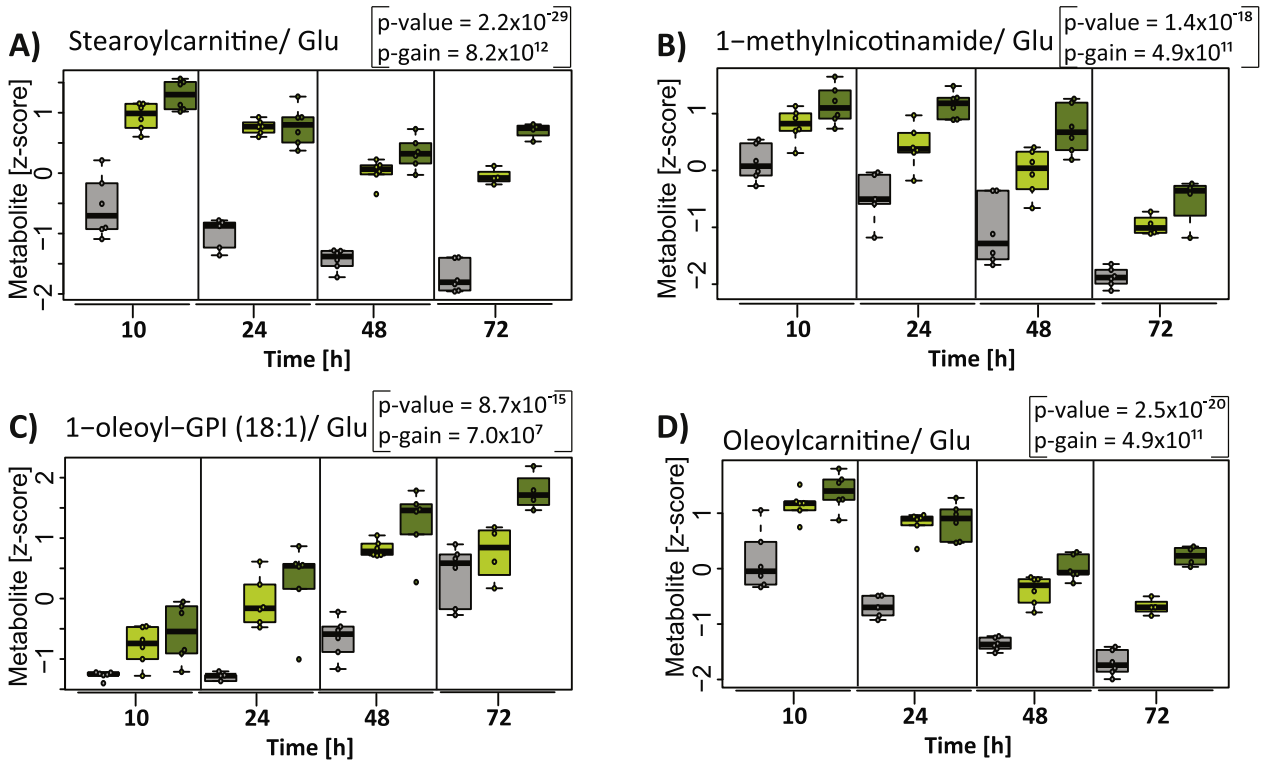

Fig. 4. Inhibition of glutaminolysis triggers an increase in ratios between molecules involved in lipid metabolism and glutamate. The boxplot presents significant alterations in the metabolic ratios of glutamate, which were observed over the entire experimental period after cell treatment with C.968. Vehicle-treated cells are depicted in grey, and those treated with 5 μM or 10 μM C.968 are indicated by green and dark green, respectively.

at later times (Supplementary Fig. 3, summarized in Fig. 5A).

Accumulation of acyl-carnitines carrying long-chain fatty acids can result from either an increase in beta-oxidation or a deficiency in carnitine palmitoyltransferase (CPT) II, the enzyme that catalyzes removal of the carnitine and simultaneous coupling of coenzyme A, the triggering step for beta-oxidation of fatty acids in mitochondria. To address the latter possibility, we assessed the relative abundance of both CPT1A and CPT2 by western blot analysis over a period of 72 h after cell treatment with C.968 (quantified at 10 h, 24 h, 48 h, and 72 h). GAC inhibition did not result in any detectable change in levels of CPT1A or CPT2 (Fig. 5B), indicating that beta-oxidation was accelerated in the MB-MDA-231 cells as a response to C.968 treatment.

We next sought to quantify the extent to which MB-MDA-231 cells use fatty acids as an energy source. To test this, we performed a fatty acid oxidation (FAO) assay using a Seahorse fluxometer (Agilent Technology). Toward this end, mitochondrial OCR was measured as a readout of FAO after incubation of cells in media supplemented with bio-available palmitate as the sole bioenergetics fuel source. To confirm that the OCR quantified in this study was specially used for FAO, we inhibited CPT-1, the rate-limiting enzyme required for FAO, with the selective inhibitor etomoxir (ETO). A higher level of basal and maximal OCR in untreated cells vs. ETO-treated cells confirmed that MB-MDA-231 cell could use FAs as a source of energy (Fig. 5C). Moreover, we observed a significant increase in cellular acetyl-CoA levels, the final product of beta-oxidation, over the experimental period (Fig. 5D).

Activation of lipid catabolism in response to glutaminolysis inhibition might suggest that lipid catabolism is a cancer cell survival mechanism. To test this possibility we further investigated whether simultaneous inhibition of glutaminolysis and FAO will have an impact on cell viability. The cells were simultaneously treated with C.968 and trimetazidine, a known beta-oxidation inhibitor [31]. We observed significant decrease in cell viability after combined treatment, with the strongest effect at 72 h (Fig. 5E).

Collectively, these results demonstrate that lipid catabolism is accelerated in response to GAC inhibition, further suggesting that under substrate-limiting conditions, lipid catabolism is accelerated to compensate for loss of energy and to contribute to the TCA cycle in the form of acetyl-CoA.

3.5. *Autophagy is triggered to protect cells from death after glutaminolysis inhibition*

Lipid catabolism was previously recognized as an important alternative source of energy for cancer cells [7] and has been associated with autophagy activation [32,33]. A role for autophagy in protecting cancer cells from death under oxidative stress, as well as nutrition insufficiency, is well known [34]. Because we observed decreased levels of the critical cellular antioxidant glutathione (GSH) following cell treatment with C.968, this result suggests GAC inhibition–mediated oxidative stress (Fig. 3 A). In support of this possibility, we showed a significantly diminished ratio of reduced glutathione (GSH to oxidized glutathione) (GSSG), providing a direct readout of C.968 treatment–induced oxidative stress (Fig. 6A). Some products of oxidative stress are highly reactive and can chemically modify the cell membrane bilayer by causing peroxidation of polyunsaturated fatty acids (PUFA), leading to formation of lipid hydroperoxides such as 4-hydroxynonenal (4-HNE), as primary products [35]. In accordance with GAC inhibition–induced oxidative stress, we observed an increase in 4-hydroxy-nonenal-glutathione, the glutathione conjugate of 4-HNE (see Fig. 6B). Together, these findings strongly indicate that MB-MDA-231 cells experience oxidative stress in response to GAC inhibition.

The observation of accelerated lipid catabolism, together with oxidative stress that is not associated with apoptosis or cell cycle aberrations, suggested that cell autophagy may be activated as a driver of lipid catabolism and thus bioenergetics fuel, protecting GAC-inhibited cancer cells from death. During autophagy, the cytosolic form of microtubule-associated protein 1 A/1B-light chain 3 (LC3-I) is converted to LC3-II, providing a molecular marker for monitoring the extent of autophagy

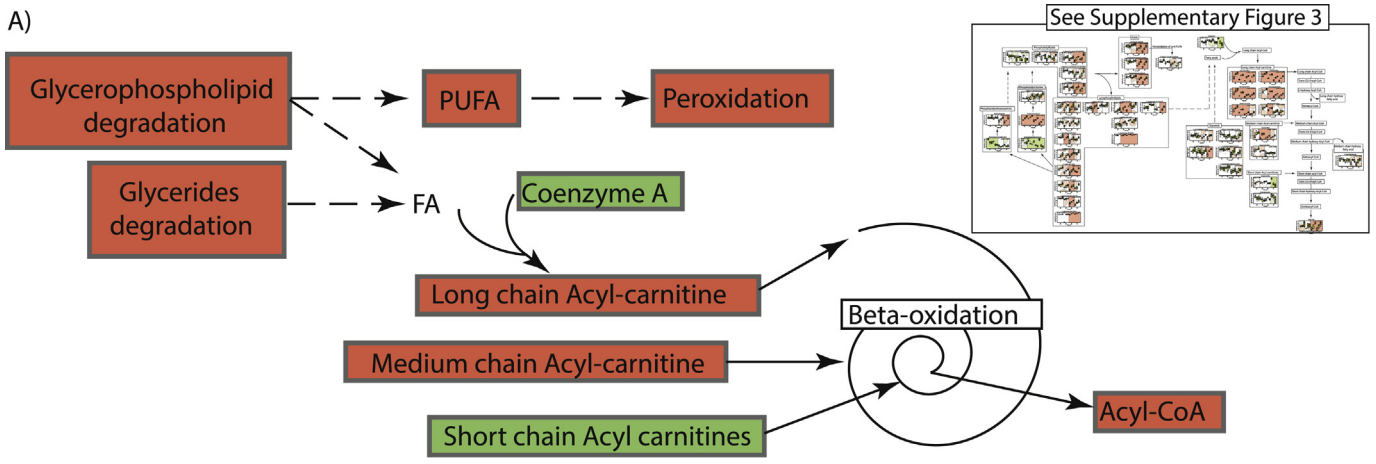

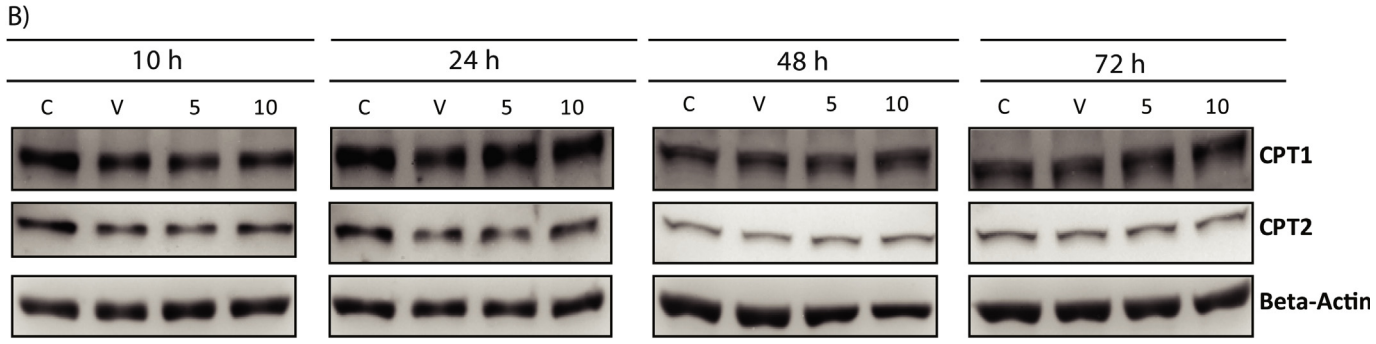

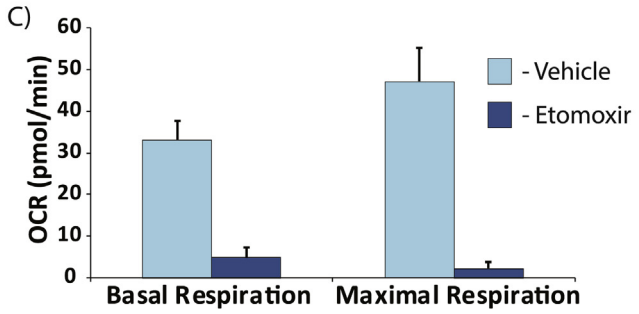

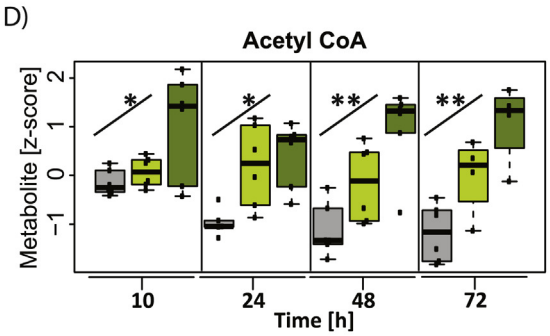

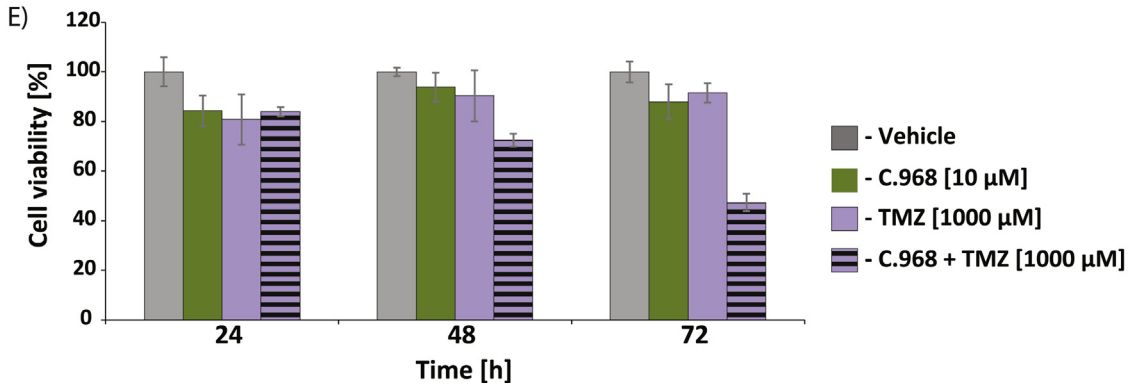

Fig. 5. Lipid catabolism is accelerated after glutaminase inhibition. A) Overview of lipid metabolism alterations after treatment of MB-MDA-231 cells with C.968. Orange – increase; green – decrease. **B)** Western blot of CPT1A and CPT2. **C)** Basal and maximal OCR were monitored in untreated cells and cells treated with CPT1 inhibitor [etomoxir (ETO)] after cell incubation in medium supplemented with bio-available palmitate. **D)** Boxplot showing significant increase in acetyl-CoA, a final product of beta-oxidation. **E)** Cell viability determined with MTT assay. Grey, vehicle-treated cells; green, cells treated with 10 µM C.968; violet, cells treated with trimetazidine (1000 µM); violet -striped, cells treated with 10 µM C.968 and trimetazidine (1000 µM). Light blue, vehicle-treated cells at basal oxidation; dark blue, etomoxir-treated cells; grey, vehicle-treated; green, 5 µM C.968–treated cells; dark green, 10 µM C.968–treated cells. *, trend to increase (p-value ≤ 0.05) at the specified time point; **, Bonferroni-corrected significant alteration (p-value ≤ 1.35 × 10–04) at the specified time point.

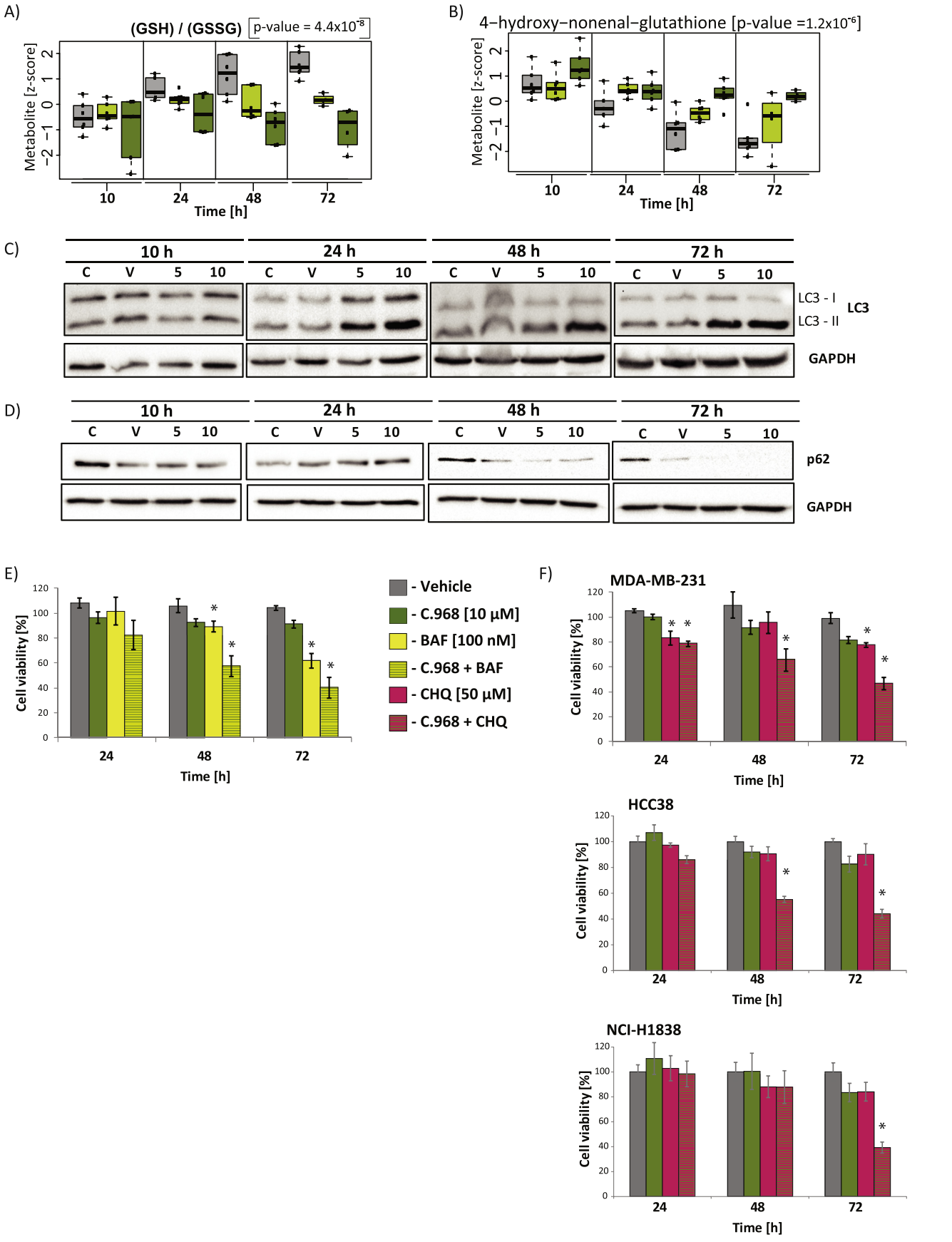

(caption on next page)

Fig. 6. Inhibition of GAC and autophagy triggers cancer cell death. A) Boxplot showing significant decrease in ratio between glutathione reduced (GSH) and glutathione oxidized (GSSG), which was observed over the entire experimental period. The p-value reflects significant changes observed after cell treatment with 10 μM drug concentration over time. **B)** Boxplots showing alteration in 4-hydroxy-noneal-glutathione, byproduct of reactive oxygen species targeting n-6 fatty acid. **C)** Western blot for LC3-I and LC3-II after treatment of MB-MDA-231 cells with C.968 at different time points. **D)** Western blot for p62 after treatment of MB-MDA-231 cells with C.968 at different time points. **E, F)** Cell viability determined with MTT assay. Grey, vehicle-treated cells; green, cells treated with 10 μM C.968; yellow, cells treated with bafilomycin (100 nM); greenish-yellow, cells treated with 10 μM C.968 and bafilomycin (100 nM); pink, cells treated with chloroquine (100 μM); greenish-pink, cells treated with 10 μM C.968 and chloroquine (100 μM). Significant changes between control and autophagy-treated cells and control and cells treated with GAC and autophagy inhibitors is indicated by *.

activation [36]. Our results reveal an increase in LC3-II 24 h after GAC inhibitor treatment, with prominent effects at 48 h and 72 h post-treatment in MB-MDA-231 (Fig. 6C). We replicated our those results in two additional cell lines including breast cancer HCC38 and lung cancer NCI-H1838. We observed increase in LC3-II abundance at 72 h after treatment in HCC38 and NCI-H1838 cancer cell lines (Supplementary Fig. 4).

Activation of the autophagy machinery is also associated with decline in p62 (sequestosome-1) protein levels, selectively degraded by autophagy [37]. Consistent with glutaminase inhibition-induced autophagy, we observed a decrease in the level of p62 in MB-MDA-231 cells after treatment with C.968 for 48 h and 72 h (Fig. 6D). These results demonstrate that C.968 treatment induces autophagy in different cancer cell lines.

3.6. Simultaneous inhibition of glutaminolysis and autophagy increases cancer cell death

We next considered the possibility that simultaneous inhibition of GAC and autophagy increases cancer cell death. To test this hypothesis, we studied the actions of two potent autophagy inhibitors, chloroquine and bafilomycin A1 [38]. Chloroquine is an US Food and Drug Administration approved drug for treatment of malaria and inhibits autophagic degradation in the lysosomes [39], whereas bafilomycin inhibits autophagy by blocking fusion between autophagosome and lysosome [40]. The viability of MB-MDA-231 cells was monitored after simultaneous inhibition of GAC with 10 μM C.968 in combination with bafilomycin (100 μM) (Fig. 6E) or chloroquine (50 nM) (Fig. 6F). . We observed that combined GAC/autophagy inhibitor treatment of MB-MDA-231 results in a significantly greater decrease in cell viability than observed with any single agent. The strongest decrease in cell viability was observed at 72 h after treatment. We further showed that combined treatment with GAC/autophagy inhibitor effectively decreases viability of other cancer cell lines including the triple negative breast cancer cell line HCC38 and the non-small cell lung cancer cell line NCI-H1838. We observed a significant decrease in the viability of HCC38 cells already 48 h after treatment with strongest effect at 72 h, whereas the viability of NCI-H1838 cells showed a significant decrease first 72 h after treatment (Fig. 6F). These findings demonstrate that combination therapy with inhibitors of both GAC and autophagy can substantially reduce cancer cell viability.

4. Discussion

Addiction of cancer cells to glutamine and increased glutaminolysis have been recognized as promising targets for selective cancer treatment [3]. This possibility is supported by the effective anti-proliferative effect of GAC inhibition by C.968 on cancer cells, with little or no effect on normal cells [18,19], and has been confirmed in a study with a different glutaminolysis inhibitor (CB-839) that recently entered a phase I clinical trial for cancer therapy [41]. However, inactivation of a single metabolic pathway in a highly complex metabolic network may be insufficient to trigger cancer cell death due to metabolic compensations, as observed for other monotherapies [42]. In this study, we showed that C.968 can suppress the proliferation of MB-MDA-231 cells, in agreement with a previous report [18]; however, this treatment failed to induce apoptotic or necrotic cell death over the experimental period. Thus, we hypothesized that compensatory metabolic alterations in response to glutaminolysis inhibition may contribute critically to cell survival.

Subsequently, metabolome-wide profiling, applied to monitor metabolic consequences of inhibited glutaminolysis, and led us to identify compensatory metabolic pathways that contribute to cancer cell survival. Our observation of accelerated lipid catabolism, as a major energy-providing pathway activated under glutaminolysis inhibition, agrees with previous studies showing that under conditions of metabolic stresses (e.g. hypoxia or nutrition shortage) cancer cells can retain viability by oxidizing lipids [43,44]. Additionally, we showed that simultaneous inhibition of glutaminolysis and lipid catabolism decreases cell viability, which to our knowledge was not previously reported. Noteworthy, inhibition of lipolysis has been shown to sensitize resistant lung adenocarcinoma to chemotherapy [45], suggesting that fatty acid oxidation is indeed a metabolic pathway that contributes to cancer cell resistance [7]. Our metabolic profiling provides further evidence that lipid catabolism, triggered in response to inhibited glutaminolysis, is a potential cancer “survival mechanism” as we further confirmed by showing accelerated cell death after simultaneous inhibition of glutaminolysis and fatty acid oxidation.

Lipid catabolism is regulated by autophagy [33]. Additionally, autophagy promotes cancer survival by recycling intracellular proteins and organelles under conditions like oxidative stress or deprivation of nutrients [46,47], thereby sustaining anabolism and enabling overall metabolic homeostasis [48]. Here we showed that shift toward lipid catabolism, under inhibited glutaminolysis, was accompanied by increased oxidative stress. We further confirmed that autophagy is triggered by the C.968 treatment in MB-MDA-231 and we confirmed this mechanism in two other cancer cell lines - lung cancer (NCi-H1838) and triple negative breast cancer (HCC38). Given that autophagy is supporting fatty acid oxidation in the mitochondria and is considered crucial for the use of fatty acids delivered from adipocytes [32,49], our observation of C.968 treatment-induced oxidative stress (Fig. 6A) and accelerated lipid catabolism (Fig. 5) suggests that activation of the autophagy pathway was triggered to protect the cells from oxidative stress and to support lipid catabolism. Noteworthy, we observed that lipid catabolism is activated prior to autophagy, which further supports the idea that autophagy is activated to support lipid catabolism.

We showed that in the case of C.968 treatment, inhibition of one metabolic pathway is not sufficient to induce cancer cell death but rather leads to the activation of alternative pathways that facilitate cancer cell survival. The mechanism identified in our study might be of relevance for clinical application, and might further contribute to our understanding why CB-839 was insufficient as single agent in clinical trial [20,21]. By inhibiting glutaminolysis and lipid catabolism or glutaminolysis and autophagy, we blocked the induced “survival mechanism,” which resulted in significantly decreased cell viability. Thus, we suggested potentially translational approach which could be further consider for clinical investigation, given that chloroquine is FDA approved drug and CB-839 was well tolerated in the phase 1 of clinical study [21]. A recent study on pancreatic ductal adenocarcinoma and colon cancer also showed that glutaminolysis inhibition activates autophagy, and simultaneous inhibition of those pathways triggered apoptosis in that setting [50,51], which corroborates our findings.

Moreover, another recent studies showed that inhibition of either autophagy or fatty acid oxidation can block tumor recurrence [52], which further suggests that a combination of therapies that simultaneously target glutaminolysis and autophagy may be beneficial.

5. Conclusions

Taken together, our study provides a framework of how a metabolome-wide profiling approach can be used to identify metabolic adjustment of cancer cells to inhibited glutaminolysis and demonstrated the feasibility of a rational approach to identify and target molecular pathways that contribute to the activation of cancer survival mechanisms. This work provides fundamental insight into cancer cell metabolic adaptations when glutamine metabolism is restricted and reveals rational targets for combination therapy.

Author contributions

Conceptualization, K.S., A.H., G.K., O.E., S.S.G., and S.U.; Investigation, A.H., M.K.; Methodology, A.H., M.K., S.B.Z., S.S.D., K.S.S., A.I., and N.J.S.; Writing and Revisions, A.H., K.S., M.K., S.U., S.B.Z, S.S.G., A.M.B, G.K., and O.E.; Funding Acquisition, K.S.; Supervision, K.S., S.S.G., G.K., and O.E.

Declarations of interest

None.

Conflicts of interest declaration

The authors declare no conflicts of interest.

Acknowledgments

This study was supported by QNRF grant NPRP8-061-3-011 and also by 'Biomedical Research Program' funds at Weill Cornell Medicine in Qatar, a program funded by the Qatar Foundation. The funders had no role in the study design, data collection and analysis, decision to publish, or preparation of the manuscript. We thank Ms. Aleksandra M. Liberska (flow cytometry supervisor) and the Flow Cytometry Facility within the Microscopy Core at Weill Cornell Medicine-Qatar for contributing to these studies.

Appendix A. Supplementary data

Supplementary data related to this article can be found at http://dx.doi.org/10.1016/j.canlet.2018.05.017.

References

[1] N.N. Pavlova, C.B. Thompson, The emerging hallmarks of cancer metabolism, Cell Metabol. 23 (2016) 27–47.
[2] O. Warburg, F. Wind, E. Negelein, The metabolism of tumors in the body, J. Gen. Physiol. 8 (1927) 519–530.
[3] B.J. Altman, Z.E. Stine, C.V. Dang, From Krebs to clinic: glutamine metabolism to cancer therapy, Nat. Rev. Canc. 16 (2016) 619–634.
[4] J.R. Mayers, M.E. Torrence, L.V. Danai, T. Papagiannakopoulos, S.M. Davidson, M.R. Bauer, A.N. Lau, B.W. Ji, P.D. Dixit, A.M. Hosios, A. Muir, C.R. Chin, E. Freinkman, T. Jacks, B.M. Wolpin, D. Vitkup, M.G. Vander Heiden, Tissue of origin dictates branched-chain amino acid metabolism in mutant Kras-driven cancers, Science 353 (2016) 1161–1165.
[5] S. Beloribi-Djefaflia, S. Vasseur, F. Guillaumond, Lipid metabolic reprogramming in cancer cells, Oncogenesis 5 (2016) e189.
[6] P. Caro, A.U. Kishan, E. Norberg, I.A. Stanley, B. Chapuy, S.B. Ficarro, K. Polak, D. Tondera, J. Gounarides, H. Yin, F. Zhou, M.R. Green, L. Chen, S. Monti, J.A. Marto, M.A. Shipp, N.N. Danial, Metabolic signatures uncover distinct targets in molecular subsets of diffuse large B cell lymphoma, Canc. Cell 22 (2012) 547–560.
[7] A. Carracedo, L.C. Cantley, P.P. Pandolfi, Cancer metabolism: fatty acid oxidation in the limelight, Nat. Rev. Canc. 13 (2013) 227–232.
[8] F. Liu, R.A. Roth, Identification of serines-967/968 in the juxtamembrane region of the insulin receptor as insulin-stimulated phosphorylation sites, Biochem. J. 298 (Pt 2) (1994) 471–477.
[9] A. Nath, C. Chan, Genetic alterations in fatty acid transport and metabolism genes are associated with metastatic progression and poor prognosis of human cancers, Sci. Rep. 6 (2016) 18669.
[10] J.H. Park, S. Vithayathil, S. Kumar, P.L. Sung, L.E. Dobrolecki, V. Putluri, V.B. Bhat, S.K. Bhowmik, V. Gupta, K. Arora, D. Wu, E. Tsouko, Y. Zhang, S. Maity, T.R. Donti, B.H. Graham, D.E. Frigo, C. Coarfa, P. Yotnda, N. Putluri, A. Sreekumar, M.T. Lewis, C.J. Creighton, L.J. Wong, B.A. Kaipparettu, Fatty acid oxidation-driven Src links mitochondrial energy reprogramming and oncogenic properties in triple-negative breast cancer, Cell Rep. 14 (2016) 2154–2165.
[12] W.W. Souba, Glutamine and cancer, Ann. Surg. 218 (1993) 715–728.
[13] N.W. Coles, R.M. Johnstone, Glutamine metabolism in Ehrlich ascites-carcinoma cells, Biochem. J. 83 (1962) 284–291.
[14] R.W. Moreadith, A.L. Lehninger, The pathways of glutamate and glutamine oxidation by tumor cell mitochondria. Role of mitochondrial NAD(P)+-dependent malic enzyme, J. Biol. Chem. 259 (1984) 6215–6221.
[15] M.I. Gross, S.D. Demo, J.B. Dennison, L. Chen, T. Chernov-Rogan, B. Goyal, J.R. Janes, G.J. Laidig, E.R. Lewis, J. Li, A.L. Mackinnon, F. Parlati, M.L. Rodriguez, P.J. Shwonek, E.B. Sjogren, T.F. Stanton, T. Wang, J. Yang, F. Zhao, M.K. Bennett, Antitumor activity of the glutaminase inhibitor CB-839 in triple-negative breast cancer, Mol. Canc. Therapeut. 13 (2014) 890–901.
[16] N. Jacque, A.M. Ronchetti, C. Larrue, G. Meunier, R. Birsen, L. Willems, E. Saland, J. Decroocq, T.T. Maciel, M. Lambert, L. Poulain, M.A. Hospital, P. Sujobert, L. Joseph, N. Chapuis, C. Lacombe, I.C. Moura, S. Demo, J.E. Sarry, C. Recher, P. Mayeux, J. Tamburini, D. Bouscary, Targeting glutaminolysis has antileukemic activity in acute myeloid leukemia and synergizes with BCL-2 inhibition, Blood 126 (2015) 1346–1356.
[17] L.A. Timmerman, T. Holton, M. Yuneva, R.J. Louie, M. Padro, A. Daemen, M. Hu, D.A. Chan, S.P. Ethier, L.J. van 't Veer, K. Polyak, F. McCormick, J.W. Gray, Glutamine sensitivity analysis identifies the xCT antiporter as a common triple-negative breast tumor therapeutic target, Canc. Cell 24 (2013) 450–465.
[18] J.B. Wang, J.W. Erickson, R. Fuji, S. Ramachandran, P. Gao, R. Dinavahi, K.F. Wilson, A.L. Ambrosio, S.M. Dias, C.V. Dang, R.A. Cerione, Targeting mitochondrial glutaminase activity inhibits oncogenic transformation, Canc. Cell 18 (2010) 207–219.
[19] C.A. Stalnecker, S.M. Ulrich, Y. Li, S. Ramachandran, M.K. McBrayer, R.J. DeBerardinis, R.A. Cerione, J.W. Erickson, Mechanism by which a recently discovered allosteric inhibitor blocks glutamine metabolism in transformed cells, Proc. Natl. Acad. Sci. U. S. A. 112 (2015) 394–399.
[20] R.M. Thompson, D. Dytfeld, L. Reyes, R.M. Robinson, B. Smith, Y. Manevich, A. Jakubowiak, M. Komarnicki, A. Przybylowicz-Chalecka, T. Szczepaniak, A.K. Mitra, B.G. Van Ness, M. Luczak, N.G. Dolloff, Glutaminase inhibitor CB-839 synergizes with carfilzomib in resistant multiple myeloma cells, Oncotarget 8 (2017) 35863–35876.
[21] D.T. Vogl, A. Younes, K. Stewart, K.W. Orford, M. Bennett, D. Siegel, J.G. Berdeja, Phase 1 study of CB-839, a first-in-class, glutaminase inhibitor in patients with multiple myeloma and lymphoma, Blood 126 (2015) 3059.
[22] A. Halama, N. Riesen, G. Moller, M. Hrabe de Angelis, J. Adamski, Identification of biomarkers for apoptosis in cancer cell lines using metabolomics: tools for individualized medicine, J. Intern. Med. 274 (2013) 425–439.
[23] A. Hansler, Q. Chen, Y. Ma, S.S. Gross, Untargeted metabolite profiling reveals that nitric oxide biosynthesis is an endogenous modulator of carotenoid biosynthesis in Deinococcus radiodurans and is required for extreme ionizing radiation resistance, Arch. Biochem. Biophys. 589 (2016) 38–52.
[24] A.M. Evans, C.D. DeHaven, T. Barrett, M. Mitchell, E. Milgram, Integrated, non-targeted ultrahigh performance liquid chromatography/electrospray ionization tandem mass spectrometry platform for the identification and relative quantification of the small-molecule complement of biological systems, Anal. Chem. 81 (2009) 6656–6667.
[25] A. Halama, M. Horsch, G. Kastenmuller, G. Moller, P. Kumar, C. Prehn, H. Laumen, H. Hauner, M. Hrabe de Angelis, J. Beckers, K. Suhre, J. Adamski, Metabolic switch during adipogenesis: from branched chain amino acid catabolism to lipid synthesis, Arch. Biochem. Biophys. 589 (2016) 93–107.
[26] K.S. Siveen, N. Mustafa, F. Li, R. Kannaiyan, K.S. Ahn, A.P. Kumar, W.J. Chng, G. Sethi, Thymoquinone overcomes chemoresistance and enhances the anticancer effects of bortezomib through abrogation of NF-kappaB regulated gene products in multiple myeloma xenograft mouse model, Oncotarget 5 (2014) 634–648.
[27] A.R. Hussain, N.A. Al-Jomah, A.K. Siraj, P. Manogaran, K. Al-Hussein, J. Abubaker, L.C. Platanias, K.S. Al-Kuraya, S. Uddin, Sanguinarine-dependent induction of apoptosis in primary effusion lymphoma cells, Canc. Res. 67 (2007) 3888–3897.
[28] E. Altmaier, S.L. Ramsay, A. Graber, H.W. Mewes, K.M. Weinberger, K. Suhre, Bioinformatics analysis of targeted metabolomics–uncovering old and new tales of diabetic mice under medication, Endocrinology 149 (2008) 3478–3489.
[29] A.K. Petersen, J. Krumsiek, B. Wagele, F.J. Theis, H.E. Wichmann, C. Gieger, K. Suhre, On the hypothesis-free testing of metabolite ratios in genome-wide and metabolome-wide association studies, BMC Bioinf. 13 (2012) 120.
[30] W.P. Katt, S. Ramachandran, J.W. Erickson, R.A. Cerione, Dibenzophenanthridines as inhibitors of glutaminase C and cancer cell proliferation, Mol. Canc. Therapeut. 11 (2012) 1269–1278.
[31] V.B. Andela, S. Altuwaijri, J. Wood, R.N. Rosier, Inhibition of beta-oxidative respiration is a therapeutic window associated with the cancer chemo-preventive activity of PPARgamma agonists, FEBS Lett. 579 (2005) 1765–1769.
[32] Y.A. Wen, X. Xing, J.W. Harris, Y.Y. Zaytseva, M.I. Mitov, D.L. Napier, H.L. Weiss, B. Mark Evers, T. Gao, Adipocytes activate mitochondrial fatty acid oxidation and

autophagy to promote tumor growth in colon cancer, Cell Death Dis. 8 (2017) e2593.
[33] R. Singh, S. Kaushik, Y. Wang, Y. Xiang, I. Novak, M. Komatsu, K. Tanaka, A.M. Cuervo, M.J. Czaja, Autophagy regulates lipid metabolism, Nature 458 (2009) 1131–1135.
[34] J.M.M. Levy, C.G. Towers, A. Thorburn, Targeting autophagy in cancer, Nat. Rev. Canc. 17 (2017) 528–542.
[35] A. Ayala, M.F. Munoz, S. Arguelles, Lipid peroxidation: production, metabolism, and signaling mechanisms of malondialdehyde and 4-hydroxy-2-nonenal, Oxid. Med. Cell Longev. 2014 (2014) 360438.
[36] Y. Kabeya, N. Mizushima, T. Ueno, A. Yamamoto, T. Kirisako, T. Noda, E. Kominami, Y. Ohsumi, T. Yoshimori, LC3, a mammalian homologue of yeast Apg8p, is localized in autophagosome membranes after processing, EMBO J. 19 (2000) 5720–5728.
[37] G. Bjorkoy, T. Lamark, A. Brech, H. Outzen, M. Perander, A. Overvatn, H. Stenmark, T. Johansen, p62/SQSTM1 forms protein aggregates degraded by autophagy and has a protective effect on huntingtin-induced cell death, J. Cell Biol. 171 (2005) 603–614.
[38] Y.P. Yang, L.F. Hu, H.F. Zheng, C.J. Mao, W.D. Hu, K.P. Xiong, F. Wang, C.F. Liu, Application and interpretation of current autophagy inhibitors and activators, Acta Pharmacol. Sin. 34 (2013) 625–635.
[39] C.A. Homewood, D.C. Warhurst, W. Peters, V.C. Baggaley, Lysosomes, pH and the anti-malarial action of chloroquine, Nature 235 (1972) 50–52.
[40] A. Yamamoto, Y. Tagawa, T. Yoshimori, Y. Moriyama, R. Masaki, Y. Tashiro, Bafilomycin A1 prevents maturation of autophagic vacuoles by inhibiting fusion between autophagosomes and lysosomes in rat hepatoma cell line, H-4-II-E cells, Cell Struct. Funct. 23 (1998) 33–42.
[41] K. Garber, Cancer anabolic metabolism inhibitors move into clinic, Nat. Biotechnol. 34 (2016) 794–795.
[42] J.S. Lopez, U. Banerji, Combine and conquer: challenges for targeted therapy combinations in early phase trials, Nat. Rev. Clin. Oncol. 14 (2017) 57–66.
[43] J.J. Kamphorst, J.R. Cross, J. Fan, E. de Stanchina, R. Mathew, E.P. White, C.B. Thompson, J.D. Rabinowitz, Hypoxic and Ras-transformed cells support growth by scavenging unsaturated fatty acids from lysophospholipids, Proc. Natl. Acad. Sci. U. S. A. 110 (2013) 8882–8887.
[44] R.M. Young, D. Ackerman, Z.L. Quinn, A. Mancuso, M. Gruber, L. Liu, D.N. Giannoukos, E. Bobrovnikova-Marjon, J.A. Diehl, B. Keith, M.C. Simon, Dysregulated mTORC1 renders cells critically dependent on desaturated lipids for survival under tumor-like stress, Genes Dev. 27 (2013) 1115–1131.
[45] J. Li, S. Zhao, X. Zhou, T. Zhang, L. Zhao, P. Miao, S. Song, X. Sun, J. Liu, X. Zhao, G. Huang, Inhibition of lipolysis by mercaptoacetate and etomoxir specifically sensitize drug-resistant lung adenocarcinoma cell to paclitaxel, PLoS One 8 (2013) e74623.
[46] E. White, Deconvoluting the context-dependent role for autophagy in cancer, Nat. Rev. Canc. 12 (2012) 401–410.
[47] H.W.S. Tan, A.Y.L. Sim, Y.C. Long, Glutamine metabolism regulates autophagy-dependent mTORC1 reactivation during amino acid starvation, Nat. Commun. 8 (2017) 338.
[48] N. Mizushima, M. Komatsu, Autophagy: renovation of cells and tissues, Cell 147 (2011) 728–741.
[49] J.Y. Guo, G. Karsli-Uzunbas, R. Mathew, S.C. Aisner, J.J. Kamphorst, A.M. Strohecker, G. Chen, S. Price, W. Lu, X. Teng, E. Snyder, U. Santanam, R.S. Dipaola, T. Jacks, J.D. Rabinowitz, E. White, Autophagy suppresses progression of K-ras-induced lung tumors to oncocytomas and maintains lipid homeostasis, Genes Dev. 27 (2013) 1447–1461.
[50] J.W. Seo, J. Choi, S.Y. Lee, S. Sung, H.J. Yoo, M.J. Kang, H. Cheong, J. Son, Autophagy is required for PDAC glutamine metabolism, Sci. Rep. 6 (2016) 37594.
[51] J. Li, P. Song, L. Zhu, N. Aziz, Q. Zhou, Y. Zhang, W. Xu, L. Feng, D. Chen, X. Wang, H. Jin, Synthetic lethality of glutaminolysis inhibition, autophagy inactivation and asparagine depletion in colon cancer, Oncotarget 8 (2017) 42664–42672.
[52] A. Viale, P. Pettazzoni, C.A. Lyssiotis, H. Ying, N. Sanchez, M. Marchesini, A. Carugo, T. Green, S. Seth, V. Giuliani, M. Kost-Alimova, F. Muller, S. Colla, L. Nezi, G. Genovese, A.K. Deem, A. Kapoor, W. Yao, E. Brunetto, Y. Kang, M. Yuan, J.M. Asara, Y.A. Wang, T.P. Heffernan, A.C. Kimmelman, H. Wang, J.B. Fleming, L.C. Cantley, R.A. DePinho, G.F. Draetta, Oncogene ablation-resistant pancreatic cancer cells depend on mitochondrial function, Nature 514 (2014) 628–632.